ISSN 0010-9525, Cosmic Research, 2017, Vol. 55, No. 4, pp. 290–305. © Pleiades Publishing, Ltd., 2017.
Original Russian Text © G.S. Zaslavskii, M.V. Zakhvatkin, N.S. Kardashev, Yu.Yu. Kovalev, E.A. Mikhailov, M.V. Popov, K.V. Sokolovskii, V.A. Stepan'yants, A.G. Tuchin, 2017, published in Kosmicheskie Issledovaniya, 2017, Vol. 55, No. 4, pp. 305–320.

Designing Corrections for the Trajectory of the *Spektr-R* Spacecraft in the Event of Immersions into the Moon's Sphere of Influence

G. S. Zaslavskii[a], *, M. V. Zakhvatkin[a], N. S. Kardashev[b], Yu. Yu. Kovalev[b], E. A. Mikhailov[c], M. V. Popov[b], K. V. Sokolovskii[b], V. A. Stepan'yants[a], and A. G. Tuchin[a]

[a] *Keldysh Institute of Applied Mathematics, Russian Academy of Sciences, Moscow, 125047 Russia*
[b] *Astrospace Center of the Lebedev Physical Institute of the Russian Academy of Sciences, Moscow, 117997 Russia*
[c] *Federal State Unitary Enterprise Lavochkin Research and Production Association, Khimki, Moscow Region, 141400 Russia*
**e-mail: zaslav@kiam1.rssi.ru*

Received February 27, 2017

Abstract—The results of updating the parameters of motion of the *Spektr-R* spacecraft at the end of 2016 have shown that, in January 2018, with a probability close to unity, the condition that a spacecraft stay in the Earth's shadow is violated; however, in May of the same year, the ballistic life of the spacecraft will be terminated. Thus, in 2017, the question arose of how to design the correction of flight of this spacecraft using its onboard propulsion system. The correction was designed with allowance for the fact that, for the first time since it was launched, the spacecraft in the course of several years, beginning with 2017, repeatedly approaches the Moon, deeply immersing into its sphere of influence. This paper presents the technologically and organizationally convenient, allowable versions of upcoming correction of the *Spektr-R* spacecraft trajectory and justifies the particular scheme of its implementation.

DOI: 10.1134/S0010952517040050

1. INTRODUCTION

The first, and still unique, correction of the *Spektr-R* spacecraft trajectory of motion (the RadioAstron project [1–4)]) was performed in February–March 2012 [5–7], less than one year after it was launched into the so-called working orbit (WO) of the artificial Earth satellite (AES) on July 18, 2011. The correction provided, for each trajectory from the set (tube) of possible trajectories of further spacecraft flight, the ballistic life of the spacecraft, the fulfillment of requirements on the light-shadow situation on spacecraft board [7], at least for the period to the beginning of 2017, and, therefore, this correction ensured the necessary conditions for implementing the research program of the RadioAstron project during this period [1, 8–19].

The central trajectory of the tube (the calculated trajectory after correction) corresponds to the time of ballistic life of a spacecraft until at least July 18, 2021, and the acceptable light-shadow situation on spacecraft board taking place until January 21, 2017.

In paper [7], it was shown that the ballistic characteristics of elements of the aforementioned tube hardly differed from one another until mid-2016 and began to markedly diverge after that date. This is due to the fact that, in mid-2016, the spacecraft closely approached the Earth (within the distances from planet's center of masses of 7030 to 7230 km, approximately) and, in this case, after this maneuver, the perturbation maneuver near the Earth, changes each trajectory significantly and in some peculiar manner from the considered set. As a result of correcting the motion parameters of the spacecraft with entering the trajectory measurements and telemetry data obtained in the second half of 2016, it was found that the ballistic life of a spacecraft will terminate in May 2018, and its unacceptable entry into the Earth's shadow will occur in January 2018, rather than January 2017. In this case, the spacecraft is located in shadow for about 6.4 h and in full shadow for at least 4.5 h, which is unacceptable for its further functioning. Therefore, in 2017, it became necessary to correct the spacecraft's trajectory by actuating its propulsion system (PS) according to a particular scheme. This scheme represents a pair of possible designed corrections, the earliest of which is regarded as a basic correction, while the other is a backup correction. It is assumed that the backup correction is carried out in cases when the performance of a basic correction is cancelled or when, for any reason, it did not lead to noticeable change in the spacecraft trajectory of motion. With this circumstance in mind, the characteristics of the designed corrections to space-

craft trajectory are accepted to be independent of whether the correction is basic or backup.

2. OBTAINING THE MAIN BALLISTIC PARAMETERS OF DESIGNED CORRECTIONS OF THE SPACECRAFT TRAJECTORY

Ballistic parameters of designed corrections of the trajectory of spacecraft flight over the AES orbit, which are necessary for choosing the scheme of implementing the spacecraft trajectory correction, are obtained by taking into account the technical spacecraft characteristics and a set of requirements to the trajectory of spacecraft flight (after performing the correction). These characteristics and requirements are given in [6]. The requirement to the trajectory of spacecraft flight after the designed correction (called hereinafter *the basic requirement*) is the insurance of spacecraft ballistic life in orbit and its illumination by the Sun till some specified time instant t_{con}.

Ballistic parameters of each designed correction of the spacecraft trajectory are calculated according to the two-level algorithmic scheme similar to that used in choosing the parameters of the correction session just before its implementation (see [6]). However, in the considered calculations, instead of the so-called [6] choice of correction parameters (CCP) task, another task is solved, called the choice of designed correction parameters (CDCP) task. In so doing, the designations and dimensions of quantities used in [6] are saved. Whereas in the CCP task, the magnitude V_{char} of the characteristic velocity increment due to PS operation in the trajectory correction session is a specified quantity, in the CDCP task, it assumes the values of the particular interval.

In the CDCP task, as in the CCP task, the time instant t^* of the middle of the PS operation interval (where the thrust is nonzero) is assumed to be specified in the spacecraft trajectory correction session.

The t^* value in the first place is chosen from the following condition: the angle γ between the unit vector $\mathbf{e}$ of the PS thrust and the direction from the spacecraft to the center of masses (CM) of the Sun at time instant t^* lies within the specified limits [6]. Here, it is assumed that vector $\mathbf{e}$ hardly differs in direction either from the direction of the spacecraft velocity vector at time instant t^* (thrust to acceleration) or from the direction opposite to this spacecraft velocity vector (thrust to deceleration). In addition, the choice of time instant t^* in designing the actual correction of the trajectory of spacecraft flight over the working orbit (WO) in 2017 should be performed taking into account the plans of implementing the research program of the RadioAstron project and existing large time intervals from the spacecraft launch (about 6 years) and from the termination of a previous correction (more than 5 years) to the designed correction. Generally speaking, the latter circumstance requires that the ballistic conditions for telecommunication along the Earth–board line be fulfilled, which allows one to obtain real-time data on the current technical state of instruments involved in correcting the flight trajectory of the spacecraft.

The research program of the RadioAstron project is formed based on applications from individual scientists and research groups for the upcoming annual research cycle. Each annual cycle lasts from July 1 to June 30. The fifth cycle (AO5) will begin on July 1, 2017. The announcement on the contest of science applications is released in December of each previous year. The announcement should include the information with the long-term orbit prediction for the whole upcoming annual period. In this regard, the results of calculations of ballistic characteristics of designed corrections of the spacecraft flight trajectory, presented in the paper, were completed in the first decade of November 2016, and the estimation of correction versions in the efficiency of obtaining science results in the AO5 cycle was completed in December 2016.

In accordance with the above considerations, it was decided

(1) to implement the correction in May–August 2017;

(2) to carry out calculations of ballistic parameters for the sequence of four versions of a designed correction in the following terms: the first version in May, the second version in June, the third version in July, and the fourth version in August;

(3) to ensure the visibility of the spacecraft from two Russian ground command-measurement stations (at Bear Lakes and Ussuriisk [20]) over the interval of powered (active) PS operation in the implementation of the designed correction of spacecraft trajectory, to be able to monitor the implementation of this correction in real time;

(4) between any two adjacent designed correction versions indicated above, to provide the interval of unpowered (passive) spacecraft flight with durations of about two or more revolutions, in order to be able to understand the emergency situation when the change in the trajectory after the scheduled correction session has failed and to repeat the attempt to implementing the spacecraft trajectory correction once again.

Before formulating the CDCP task, we introduced into consideration the so-called coefficient C_V of admissible variations in the characteristic velocity increment during correction. Let V_{char} be some value of this characteristic velocity increment at correction, which ensures the fulfillment of the *basic requirement* for the spacecraft flight trajectory after correction at the given value of t_{con}. Then, coefficient $C_V \geq 0$ determines the maximum-in-length segment $I_C = [1 - C_V)V_{\text{char}}, (1 + C_V)V_{\text{char}}]$ of the numerical axis, each point of which, as the value of the characteristic velocity increment at correction, ensures the fulfillment of the

above *basic requirement*. At a fixed value of the *basic requirement* to the spacecraft flight trajectory after correction, coefficient C_V represents the maximum value of relative deviations in the characteristic velocity increment at correction from the V_{char} value, for which the fulfillment of the above demand is not violated as follows:

$$C_V = C_V(t_{con}, V_{\text{char}}). \quad (1)$$

The practice of works on ballistic-navigation support (BNS) for more than 5 years of flight of the *Spektr-R* spacecraft has shown that the dominant contribution into possible deviations of the spacecraft motion trajectory after the correction is made by the error in the implementation of the constant PS thrust, the extreme value of which can reach 9% of the nominal thrust. Therefore, at the design stage of the spacecraft trajectory correction scheme, only this error is taken into account. Because the cutoff of powered operation of PS of the spacecraft under consideration occurs over time, the indicated error is almost directly transformed into similar error while implementing the magnitude of the characteristic velocity increment of the spacecraft. With this statement in mind, if the spacecraft trajectory correction is planned to be performed at given values of t_{con} and V_{char}, then with the coefficient C_V of the admissible variations in the characteristic velocity increment (which corresponds to (1)), at correction no lower than 0.09, the *basic requirement* in the trajectory after correction is fulfilled with a probability close to unity, and this probability grows with increasing coefficient C_V.

In addition, it should be noted that the V_{char} value for technical reasons must lie within the limits of the specified segment $I_{V_{\text{char}}}$ on the nonnegative part of the numerical axis

$$V_{\text{char}} \in I_{V_{\text{char}}}, \quad I_{V_{\text{char}}} = [V_{\text{char min}}, V_{\text{char max}}], \quad (2)$$

and the sought value, which gives a ballistic estimate to the predicted correction, is the maximum ($C_V^{\max}$) of function (1) on the set (2). The argument that delivers this maximum is denoted by $V_{\text{char}}^{\max}$, i.e., $C_V^{\max} = C_V(V_{\text{char}}^{\max})$. The $V_{\text{char}}^{\max}$ value is sought approximately on the finite set $M_{V_{\text{char}}}$ of points of the segment $I_{V_{\text{char}}}$ (2), which is determined by the step $h_{V_{\text{char}}}$, namely,

$$M_{V_{\text{char}}} = \{V_{\text{char min}}, V_{\text{char min}} + h_{V_{\text{char}}}, V_{\text{char min}} + 2h_{V_{\text{char}}}, \ldots, V_{\text{char min}} + qh_{V_{\text{char}}}\}, \quad (3)$$

moreover, q is the minimum nonnegative integer at which the inequality $V_{\text{char max}} + (q+1)h_{V_{\text{xap}}} > V_{\text{char max}}$ holds.

CDCP task. The following is specified: t_0, x_0, y_0, z_0, V_{x0}, V_{y0}, V_{z0}, s, and S_d are the initial conditions (ICs) of spacecraft motion, where x_0, y_0, and z_0 are the coordinates of vector $\mathbf{r}(t)$ of position and V_{x0}, V_{y0}, V_{z0} are the components of spacecraft velocity $\mathbf{V}(t)$ at the initial time instant $t = t_0$ in the $J2000$ coordinate system (CS), s is the ballistic coefficient for calculating the aerodynamic drag force in the Earth's atmosphere [6, 21], and S_d is the coefficient of light pressure on a spacecraft [6]. Here and below, it is assumed that the J2000 CS axes coincide in direction with the axes of the EME2000 barycentric coordinate system [22], and the center of the system is at the Earth's center of masses (CM); m_0 is the value of spacecraft mass m at time instant $t_{\partial n}$ of PS ignition; P is the nominal thrust of PS; I_{sp} is the specific impulse of PS; t^* is the middle of the interval of continuous PS operation in the correction session; $\mathbf{e}$ is the unit vector (in the J2000 CS) of the PS thrust direction at implementing the correction; $V_{\text{char min}}$, $V_{\text{char max}}$ are the minimum and maximum allowable values of the characteristic velocity increment as a result of PS operation (2); $h_{V_{\text{char}}}$ is the step in the value of the characteristic velocity increment, which determines (3) the set $M_{V_{\text{char}}}$; $h_{\pi c}$ is the allowable-from-below spacecraft flight altitude, which, when reached, by definition sets the time of the termination of the spacecraft's ballistic life. Here and below, when calculating the spacecraft flight altitudes the Earth figure is approximated by a sphere of radius $R_{\text{E}} = 6378$ km; h_{tc} is the step (in time) of checking the spacecraft ballistic life (fulfillment of the condition $h_\pi(t) \geq h_{\pi c}$); t_{spec} is the time until the spacecraft ballistic life is checked, $t_{\delta e} \leq t_c \leq t_{\text{spec}}$, where $t_{\partial e}$ is the PS cutoff time instant.

For each value of the characteristic velocity increment ($V_{\text{char}} \in M_{V_{\text{char}}}$) and given time instant t^* (see above), to obtain the parameters that characterize the corresponding correction of the spacecraft flight trajectory as follows:

—$\{t_{\partial e}, \mathbf{r}(t_{\partial e}), \mathbf{V}(t_{\partial e})\}$ are kinematic parameters of the spacecraft's motion in the $J2000$ CS for the time of the termination of PS operation;

—$m_e = m(t_{\partial e})$ is the spacecraft's mass at the time of the termination of PS operation calculated in accordance with Tsiolkovsii's formula $m_e = m_0 - 2P(t_{\partial e} - t^*)/I_{\text{sp}}/g_0$ (only the loss of the spacecraft's mass due to fuel consumption during corrections is taken into account), where $g_0 = 9.80665$ m/s^2;

—$t_{\partial n}$, Δt_∂ are the time instant of PS ignition for implementing the spacecraft motion correction and the duration of PS operation, respectively;

—t_{ce} is the time of the termination of the ballistic life of the spacecraft working orbit, where, if the spacecraft ballistic life is ensured before the specified time instant t_{spec}, then the following is set: $t_{ce} = t_{\text{spec}}$.

—N is the number of time segments of spacecraft shading [6, 7] that belong to the interval $[t_{\partial e}, t_{ce}]$ from the PS cutoff during the implementation of the designed correction until the completion of the ballistic life of the spacecraft's working orbit after the correction;

—$t_{\text{shad}nj}$, $t_{\text{shad}ej}$, $t_{a\text{shad}nj}$, $t_{a\text{shad}ej}$, $K_{T_{\max j}}$ is the ordered ($t_{\text{shad}n1} < t_{\text{shad}n2} < \ldots < t_{\text{shad}nN}$) sequence of values of groups of five calculated along the trajectory after correction, namely, the beginning and end of a shading time segment ($[t_{\text{shad}nj}, t_{\text{shad}ej}]$), the beginning and the end of the full Sun eclipse segment ($[t_{a\text{shad}nj}, t_{a\text{shad}ej}]$) and the degree $K_{T_{\max j}}$ of spacecraft shading on the jth shading time segment (all considered segments belong to the interval $[t_{\partial e}, t_{ce}]$);

the massif of the following parameters of a spacecraft orbit, osculating for time instant $t_{\partial e}$, after correction, in the J2000 CS: $h_\pi$is the pericenter altitude above the Earth surface h_α is the apocenter altitude above the Earth surface, ω is the pericenter latitude argument, i is the inclination, Ω is the ascending node longitude, P_o is the orbit period t_π is the time of spacecraft's passage through the orbit pericenter on the previous stage, and t_Ω is the time of spacecraft passage through the beginning of the current flight revolution.

Here and below, it is supposed that quantities ω and Ω assume the values from the half-interval $[0, 2\pi)$, and quantity i is from the interval $[0, \pi]$, the orbit revolution number is increased by unity at the time of spacecraft passage through the ascending node, i.e., when the spacecraft crosses the reference plane of the J2000 CS, and its applicate changes the sign from minus to plus.

The solution of the CDCP task is a laborious process because the high-precision numerical method must be used many times to integrate a complicated system of differential equations that describes the spacecraft's motion over the WO during long intervals (several years) of flight. However, as a result of solving this task, the solution of higher-level tasks, each of which, for any fixed basic requirement to the flight trajectory (after performing the correction) determines the values corresponding to $V_{\text{char}}^{\max}$ and $C_V^{\max}$, is reduced to the enumeration of the already obtained data.

It should be emphasized that, at the stage of flight during several years (after 2016), the spacecraft many times closely encounters the Moon, when the Earth satellite enters the sphere of its gravitational influence rather deeply [23], which will be shown in the next paraplot of this paper. Therefore, when solving the CDCP task at the considered stage, the ephemeris (the components of the vectors of position and velocity of CM) of the Moon must be calculated and taken into account to a high accuracy.

3. QUALITATIVE ESTIMATION OF THE SPACECRAFT FLIGHT TRAJECTORY UNTIL THE UPCOMING CORRECTION

The current spacecraft trajectory was formed as a result of implementing the correction in 2012. Performing flight over this trajectory, the spacecraft for the first time enters the sphere of gravitational influence of the Moon [23] in 2017. Radius R_{inf} of this sphere is approximately equal to 102000 km. This fact has been demonstrated for two trajectories (from the tube of possible trajectories after performing the correction in 2012): the trajectory *T*1*0,* which corresponds to the nominal performance of correction, and the trajectory *T*1*1,* the parameters of which were obtained by trajectory measurements in the interval of several revolutions after correction with attracting the ballistic data from the telemetry information.

Figure 1 presents by a solid thin line the plot of distance of spacecraft *DOM* from the Moon CM as a function of time of its flight over the trajectory *T*1*0,* which is counted from the time instant indicated along the abscissa axis. A similar plot is presented by the solid bold line in Fig. 2 for the case of spacecraft flight over the trajectory *T*1*1.*

The presented plots allow one to draw the following conclusions on the character of spacecraft encounters with a natural satellite of the Earth:

(1) the first (after the trajectory correction in 2012) the immersion of the spacecraft into the Moon's sphere of influence occurs upon a revolution March 2017;

(2) until April 2018, at least five spacecraft immersions into the Moon's sphere of influence occur;

(3) among these spacecraft immersions, there are deep immersions (in January–February 2018), when the spacecraft almost reaches the Moon's sphere of influence [23], the radius R_{act} of which is approximately equal to 66000 km;

(4) the configurations of spacecraft immersions into the Moon's sphere of influence for the considered flight trajectories markedly differ from each other, which, generally speaking, should further lead to the significant divergence of parameters of spacecraft flight trajectories relative to the Earth.

The last of the aforementioned conclusions is confirmed by the dependences of parameters of spacecraft trajectories on the flight time, which are illustrated in Figs. 3–7. Here and below, the trajectory parameters on each spacecraft flight revolution are as follows: $r_{\min}$ is the minimum distance of a spacecraft from the Earth's center of mass (CM), which is reached at the time instant denoted by $t_{\min}$; $r_{\max}$ is the maximum distance of a spacecraft from the Earth's CM; P_{om}, ω_m, i_m, and Ω_m, are the period, pericenter latitude argument, inclination, and the ascending node longitude of the osculating orbit at time instant $t_{\min}$, respectively.

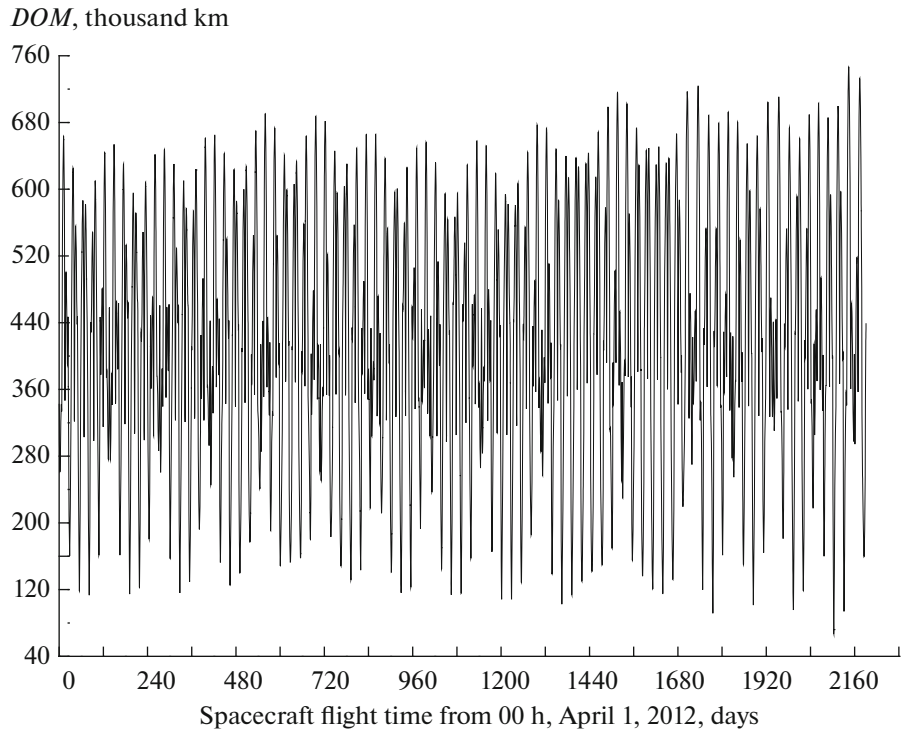
DOM, thousand km
760
680
600
520
440
360
280
200
120
40
0
240
480
720
960
1200
1440
1680
1920
2160
Spacecraft flight time from 00 h, April 1, 2012, days

Fig. 1.

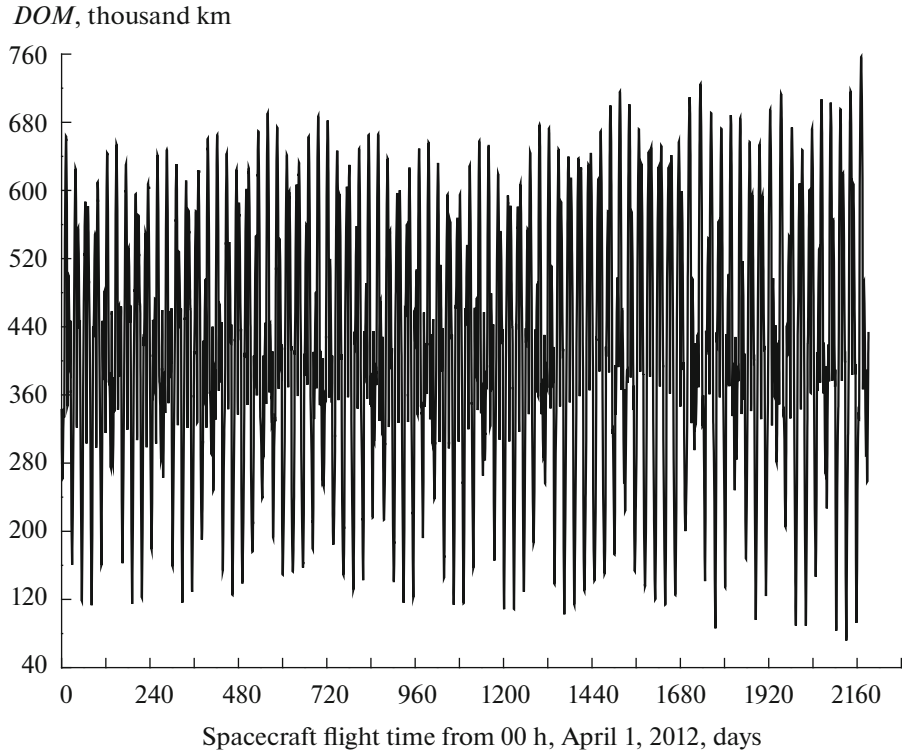
DOM, thousand km
760
680
600
520
440
360
280
200
120
40
0
240
480
720
960
1200
1440
1680
1920
2160
Spacecraft flight time from 00 h, April 1, 2012, days

Fig. 2.

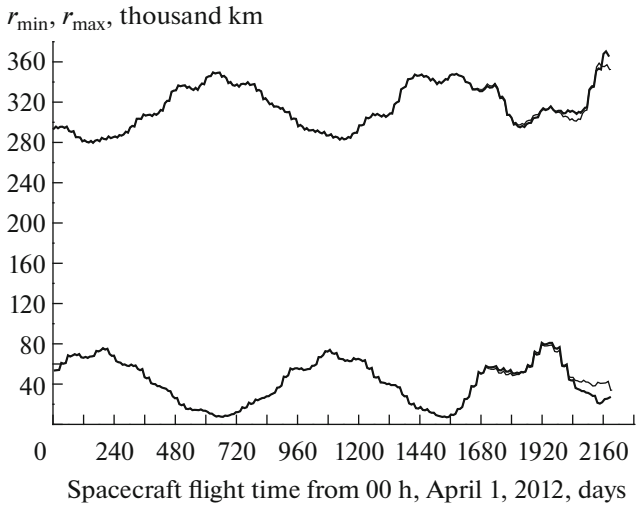

Fig. 3.

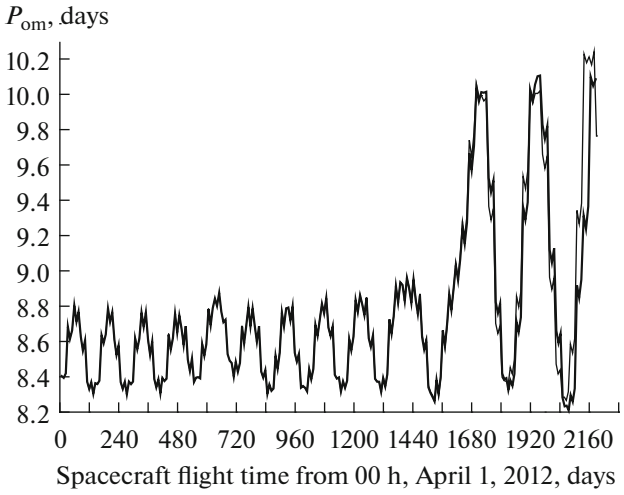

Fig. 4.

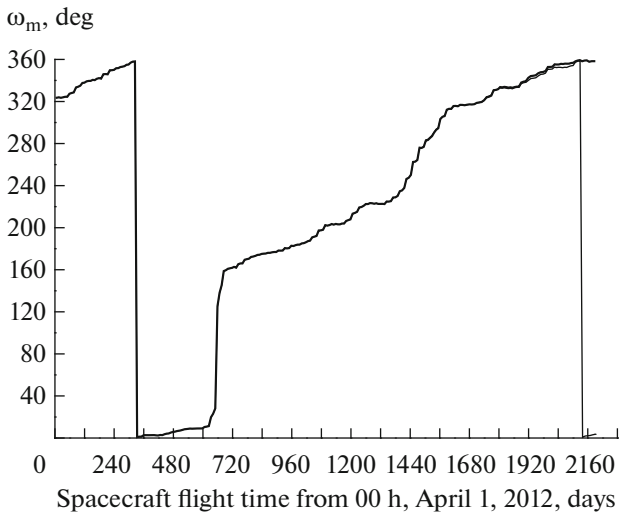

Fig. 5.

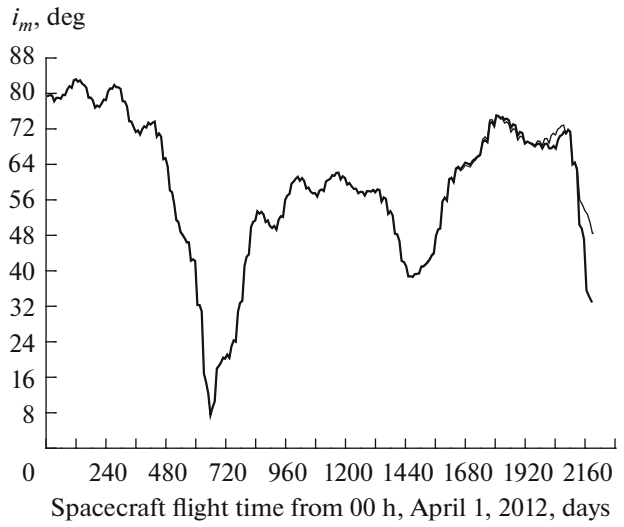

Fig. 6.

The dependence of the trajectory parameter in the figure is depicted in the form of a plot that represents a broken line. The abscissa axis of plots presents the time instants counted from the time instant indicated along this axis. The abscissas of the vertices of broken lines for parameters r_{min}, P_{om}, ω_m, i_m, and Ω_m are the time instants when the satellite reaches the minimum (on a revolution) distance from the Earth's CM and, for parameter r_{max}, they are the time instants t_{max} when the satellite reaches the maximum (in a revolution) distance from the Earth's CM of achieving maximum companion (coil) of the distance from the Earth's CM. The ordinate of the broken line vortex equals the calculated value of the parameter indicated in the figure. The plots for the *T*1*0* trajectory are depicted by a continuous thin line and, for the *T*1*1* trajectory, by a continuous thick line. They were drawn on the figure in the sequence based on the thickness of lines depicting them, i.e., thin or thick.

The information presented in Figs. 3–7 shows that the *T*1*0* and *T*1*1* trajectories hardly differ from each other up to the beginning of 2017. Then, when the spacecraft repeatedly (during several years) closely encounters the Moon's sphere of influence and even immerses into it, these trajectories begin to noticeably differ from each other. It follows from this that, in the period of rather close encounters with the Moon, one can hope that the spacecraft can be transferred (by means of correction with small fuel expenses) into flight trajectory that differs significantly from the current trajectory.

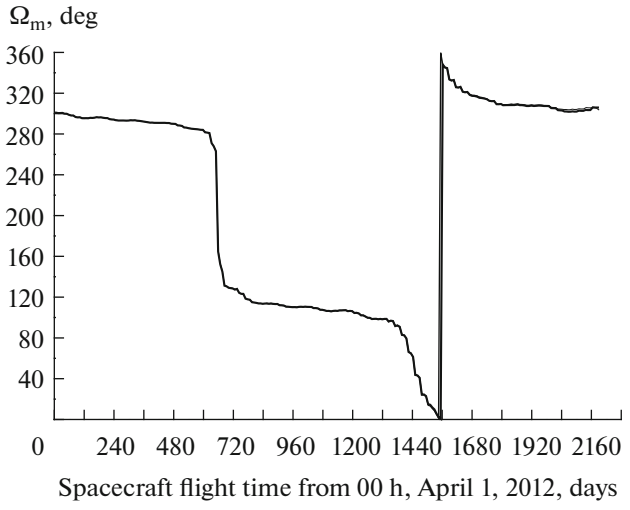

Fig. 7.

The following sections of the paper present the ballistic parameters of the four designed allowable corrections: *K21, K22, K23,* and *K24* of the spacecraft orbit, the implementation of which can be executed in May, June, July, and August 2017, respectively. These parameters are calculated for the spacecraft trajectory updated in the fourth quarter of 2016, which is called *current trajectory* and is denoted as *T*1*T*. The calculated spacecraft ballistic life on the *T*1*T* trajectory will terminate on May 21, 2018, and the first unacceptable spacecraft entering the Earth's shadow will occur on January 6, 2018.

4. VERSIONS OF THE SPACECRAFT FLIGHT TRAJECTORY CORRECTION

Each of designed *K22, K23,* and *K24* corrections, like the correction performed in 2012, is carried out in the vicinity of the time instant $t_{\max}$ of the current spacecraft flight revolution and is called a *regular correction*. As a result of this correction, the basic requirement to the trajectory of further spacecraft flight should be fulfilled. In this case the characteristic velocity increment as a result of PS operation should be close in magnitude to the minimum value. Taking into account the slow change in the position of the spacecraft and direction of the velocity in the J2000 CS in the vicinity of $t = t_{\max}$, it is almost permissible to assign time instant t^* (the middle of the interval of continuous PS operation in the regular correction session) within deviations from the time instant $t_{\max}$ of up to 8 h while maintaining the chosen PS thrust direction at time instant $t_{\max}$.

The designed *K21* correction suggests the formation of the spacecraft flight trajectory, moving over which the spacecraft repeatedly immerses into the Moon's sphere of influence, and after these immersions it, for a while (less than for a year), is transferred into the so-called rounded orbit of satellite. Quantity $r_{\min}$ on revolutions of this orbit lies in the vicinity of 100 thousands km.

Calculations of parameters of each of *K2i* corrections ($i = 1, 2, 3, 4$) is reduced to the solution of the previously considered CDCP task with similar values of initial conditions (IC), m_0, P, I_{sp}, $V_{\text{char min}}$, $V_{\text{char max}}$, $h_{V_{\text{char}}}$, $h_{\pi c}$, h_{tc} and t_{spec}. For the components of the vector of indicated ICs, we used the corresponding IC components for the current trajectory *T*1*T*.

Based on the experience of solving BNS tasks of the *Spektr-R* spacecraft flight, the values of quantities $h_{\pi c}$, h_{tc}, and t_{spec} were taken to be equal to 640 km; 5 s; and July 18, 2021, 00.00.00, respectively, and quantity $h_{V_{\text{char}}}$, taking into account the degree of spacecraft immersion into the Moon's sphere of influence, was assigned from the range of 0.02–0.05 m/s.

Based on the technical characteristics of the correction session of the *Spektr-R* spacecraft, quantities $V_{\text{char min}}$, $V_{\text{char max}}$ were taken to be equal to 0 and 10 m/s, respectively.

Table 1 presents the main characteristics of four planned spacecraft trajectory corrections. In this table (and hereafter over the text) *T*2*i* denotes the spacecraft flight trajectory in the case of error-free implementation of the designed 2nd correction in the *i*th version, $i = 1, 2, 3, 4$. All rows in the table, except the row dedicated to parameter C_V'' (see below), present characteristics of versions of corrections at the fixed time instant t_{con}, for which, after performing the correction, it is necessary to ensure that the basic requirement to the spacecraft flight trajectory, i.e., $t_{con} = t_{con}'$ = January 1, 2020, 00.00.00, is fulfilled. Here, it is assumed that $V_{\text{char}} = V_{\text{char}}^{\max}$ and, in accordance with (1), $C_V' = C_V(t_{con}', V_{\text{char}}^{\max})$. The meaning of the quantities $V_{\text{char}}^{\max}$ and C_V was outlined in detail above. The letters in parentheses after the value V_{char} indicate the direction of the thrust vector, i.e., A is acceleration and D is deceleration. The maximum value of relative deviations of the characteristic velocity increment at correction from the indicated value V_{char}, for which the fulfillment of the *basic requirement* to the spacecraft flight trajectory is not violated until the specified time instant $t_{con} = t_{con}'$ = December 15, 2018, 00.00.00, is presented in the table by quantity $C_V'' = C_V(t_{con}'', V_{\text{char}})$. Quantities $t_{\text{shad}n}$, δt_{shad}, $K_{T_{\max}}$, $t_{\text{ashad}n}$, δt_{ashad} characterize the first unacceptable spacecraft shading by the Earth after corrections. These quantities and the value of the angle γ, which was introduced into consideration earlier, were calculated under the assumption that the spacecraft moves

Table 1. Parameters of designed corrections of spacecraft motion and corresponding flight trajectories after the nominal performance of the correction

Parameter	Correction			
	K21	*K22*	*K23*	*K24*
t^*	May 21, 2017 08.59.40	June 17, 2017 09.40.00	July 16, 2017 09.30.00	August 5, 2017 09.20.00
V_{char}, m/s	5.75 (D)	3.93 (A)	1.55 (A)	0.85 (A)
γ, deg	92.50	94.90	100.95	93.28
C_V'	0.02	0.06	0.16	0.15
C_V''	0.13	0.23	0.31	0.24
t_{ce}	>July 18, 2021 00.00.00	>July 18, 2021 00.00.00	>July 18, 2021 00.00.00	>July 18, 2021 00.00.00
$t_{\text{shad}nj}$	January 16, 2020 05.50.51	>July 18, 2021 00.00.00	>July 18, 2021 00.00.00	January 8, 2020 12.56.52
$\delta t_{\text{shad}nj}$, h	5.79	–	–	6.61
$K_{T_{\max}}$	1.000	–	–	1.000
$t_{\text{ashad}nj}$	January 16, 2020 06.51.17	–	–	January 8, 2020 13.56.36
$\delta t_{\text{ashad}nj}$, h	3.74	–	–	4.55

along the trajectory after the error-free performance of the designed correction version. The absence of values of quantities δt_{shad}, $K_{T_{\max}}$, $t_{\text{ashad}n}$, δt_{ashad} in the column in Table 1 indicates the absence of inadmissible spacecraft shadings by the Earth up to the time instant t_{spec} during spacecraft's flight over the corresponding trajectory (see column). All values of angle γ presented in the table belong to the admissible range [6] for implementing the correction, i.e., 90°–165°.

Figures 8–16 present the plots of dependences of quantities *DOM*, $r_{\min}$, $r_{\max}$, P_{om}, ω_{m}, i_m, and Ω_{m} on the time of the spacecraft's flight over the trajectories *T2i* (i = 1, 2, 3, 4). The principle of constructing dependences in the form of plots is identical to the construction of similar dependences presented in Figs. 1–7. The plots in figures 12–16, which are related to the same trajectory, are depicted by particular lines as follows: *T21* corresponds to dashed lines, *T22* corresponds to discontinuous lines, *T23* corresponds to continuous thin lines, and *T24* corresponds to continuous thick lines. The plots were drawn on the figure in the sequence of lines depicting them, i.e., dashed, discontinuous, continuous thin, continuous thick.

In conclusion to this section, one should note that, in predicting the spacecraft motion over the trajectories under consideration, after the planned correction up to the time instant t_{spec}, no inadmissible spacecraft shadings by the Moon were revealed. The Moon figure was considered to be a sphere with the specified radius R_{M} = 1738 km.

5. BALLISTIC ESTIMATION OF VERSIONS OF THE PLANNED CORRECTION OF THE SPACECRAFT FLIGHT TRAJECTORY

The calculated data presented in Table 1 and Figs. 8–16 allow one to arrange (from the viewpoint of technical implementation and ballistic features) the versions *K2i* (i = 1, 2, 3, 4) of the upcoming correction of the spacecraft flight trajectory according to priority. For this purpose, it is necessary to pay attention to the following characteristics of versions.

1. The increments of the characteristic spacecraft velocity for the considered correction versions markedly differ among themselves in magnitude. Here, this magnitude (which is proportional to the fuel consumption for correction) decreases as the number of the correction version rises.

2. Correction versions *K21* and *K22* do not satisfy the *basic requirement* to the trajectory after implementation of correction up to the beginning of 2020, because for these correction versions quantities C_V' are less than the specified allowable minimum value of 0.09. However, both of them satisfy the *basic requirement* up to the middle of December 2018 because the following inequality holds for each of them: $C_V'' > 0.09$; here, the *K22* version is preferred because it has a higher value of C_V'' than the *K21* version.

3. Correction versions *K23* and *K24* satisfy the *basic requirement* to the trajectory after implementing the correction up to the beginning of 2020 because, for each of these versions of corrections, the value of quantity C_V' is greater than the value of 0.09. The *K23*

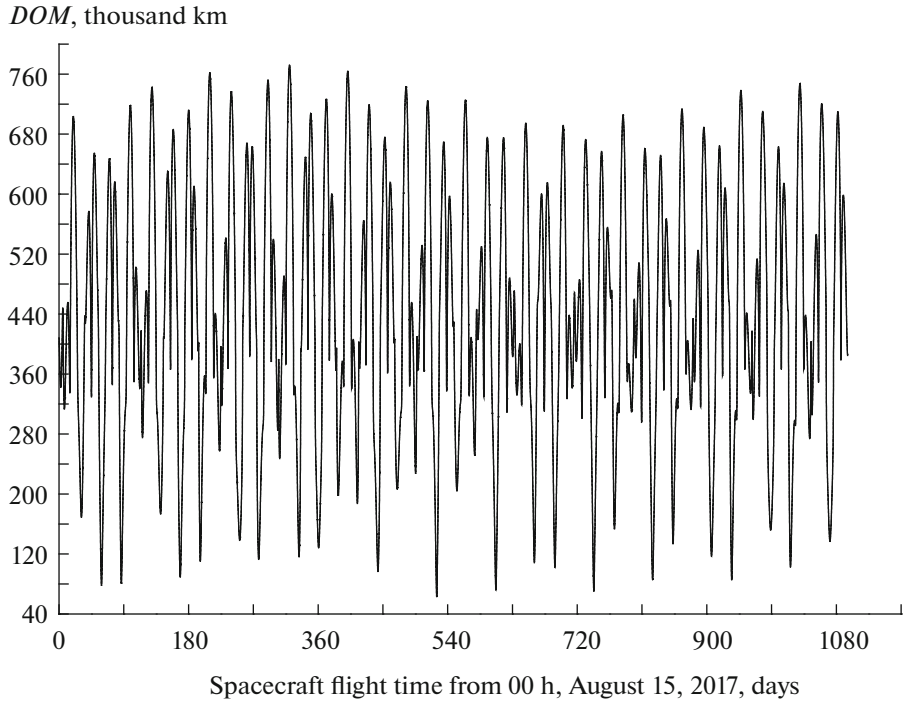

Fig. 8.

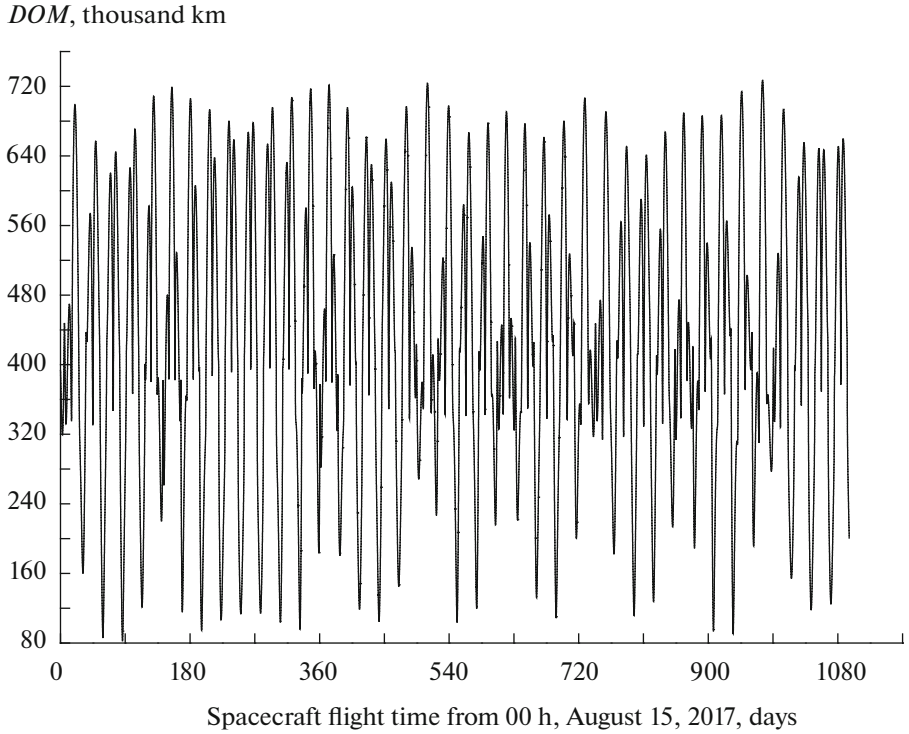

Fig. 9.

correction version is slightly preferred because it has a slightly greater value of C_V' than the *K24* version.

4. The plot in Fig. 8 indicates that, when flying over the *T21* trajectory (after the *K21* correction), the spacecraft through the middle of December 2018, the reaches the Moon's sphere of influence $DOM \approx R_{\text{inf}}$. This close encounter between the spacecraft and the Moon can lead to a drastic expan-

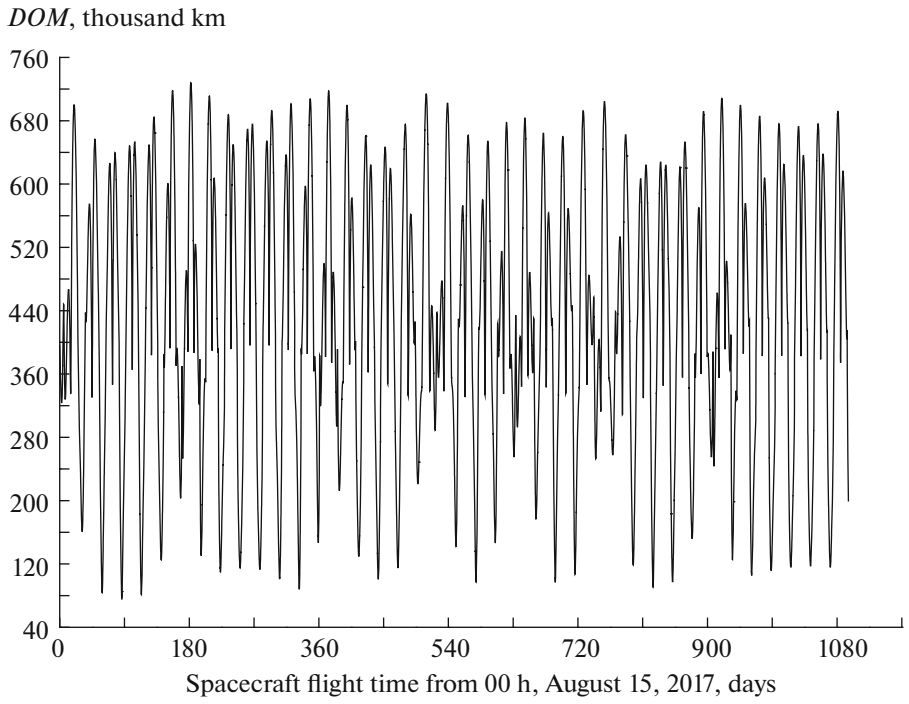

Fig. 10.

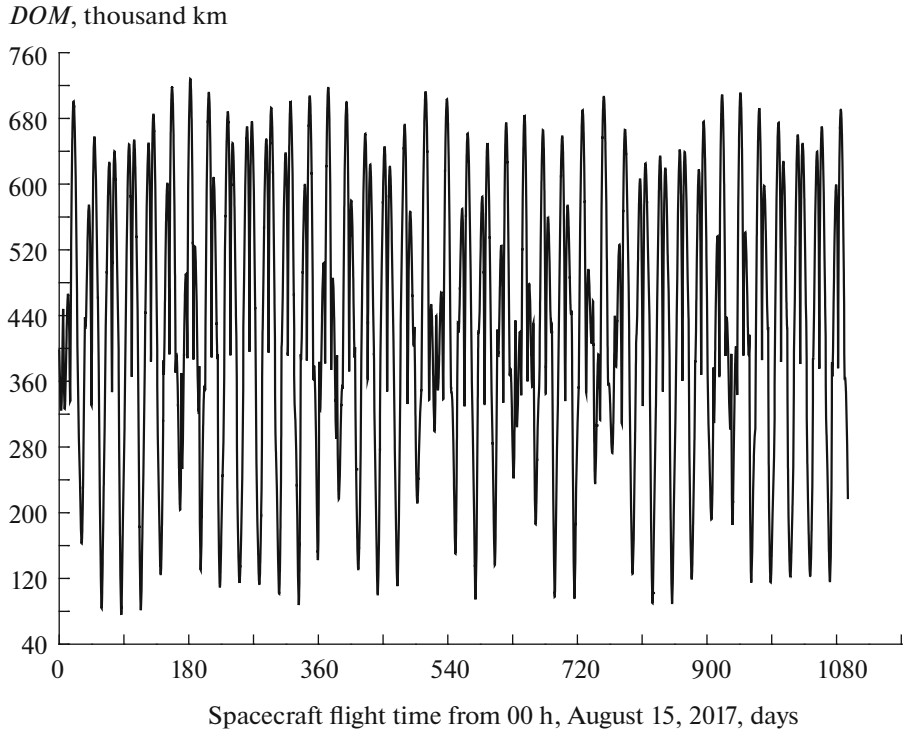

Fig. 11.

sion of the tube of possible trajectories of its further flight.

5. Based on the plots of Figs. 9–11, it can be concluded that, when the spacecraft flies over any *T22, T23,* or *T24* trajectory (after *K22*, *K23*, *K24* corrections, respectively), before the beginning of 2020, it will be located outside the Moon's sphere of influence and will only enter it a few times, i.e., $DOM < R_{act}$.

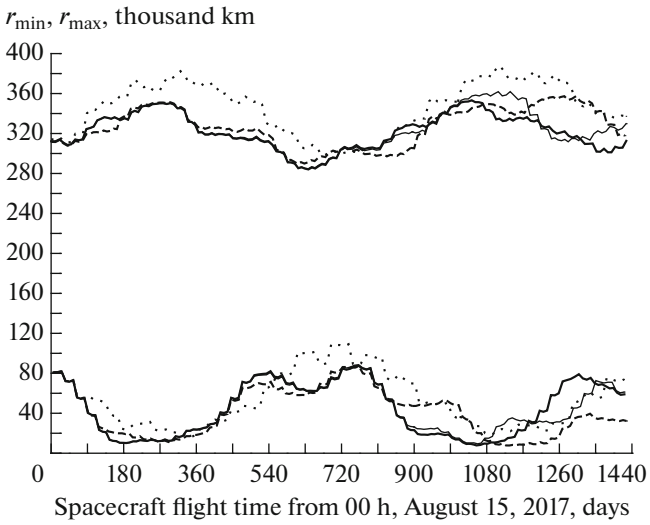

Fig. 12.

6. The plots in Figs. 12–16 show that the parameters of the *T22, T23,* and *T24* trajectories of the spacecraft's flight differ of only slightly from each other up to January 2020.

Based on the listed characteristics of the considered *K2i* versions *(i* = 1, 2, 3, 4) of the upcoming correction of the spacecraft flight trajectory, the *K23* correction seems to be the most acceptable (priority) for implementation. The *K24* correction seems to be the second choice. The *K21* and *K22* corrections have lower priorities. For these two versions of corrections, one should provide for the performance of an additional correction in 2018.

6. PLANNING OF INTERFEROMETRIC OBSERVATIONS

Planning of the observation of radio sources using a ground-space interferometer (GSI) is done taking into account a number of requirements[1] that must be followed when implementing these observations. The requirements primarily regard the following tasks:

(1) providing the technical conditions for the operation of the involved onboard hardware;

(2) ensuring the availability of the necessary visibility of the observed radio source from the space telescope (on board the *Spektr-R* spacecraft) and from a ground-based telescope;

(3) establishing a high-speed communication channel between the spacecraft and the ground-based station in Pushchino or in Green Bank to download scientific data in real time (the volume of data is too large to store on board);

(4) meeting the requirements for scientific experiment regarding the length and orientation of GSI bases.

The FakeRaT program, which is a modified version of the fakesat code (see details and references in [24]), is used to check whether the operating conditions of the space telescope's operation have been met.

The SCHED program[2] is used to calculate the conditions for the visibility of radio sources using ground-based telescopes. This program is widely used to prepare ground-based interferometric observations and contains the latest information on positions and angular limitations of radio telescopes. The scripts we have composed control the actuation of the FakeRaT and SCHED, as well as interpret the results of operation of these programs and present information about the visibility conditions in tabular form.

When working with the GSI, two basic variants of observations are used. The first variant consists of repeated short observations of the same radio source in order to construct an image of it (see, e.g., [10, 11, 17]). The total duration of this observation version is typically 8–30 h with breaks for cooling. A total of 10–40 ground-based radio telescopes in Russia, Europe, the United States, South Africa, Australia, South Korea, China, and Japan participate in the *Spektr-R* observations. The observation is carried out close to the time instant t_{min}, when the spacecraft reaches minimum distance from the Earth's CM on the flight revolution. This corresponds to two factors: (a) the minimum difference between the shortest ground-space bases and the longest ground bases, and (b) considerable change of length and orientation of ground-space bases during the observation time. Both factors are important for successful reconstruction of the image.

The second variant consists of a unique observation with durations ranging from 40 min to 2 h. The purpose of this observation to measure the interference signal amplitude, which allows one to judge the size and brightness of the observed radio source without restoring its detailed images [1, 12, 17], or the scattering parameters [8, 13–16, 18]. For observations in this mode, the support of at least one large ground-based telescope is sufficient. These observations are possible on any ground-space bases. It is important that, after implementing its correction, the spacecraft flight trajectory made it possible to perform observations of both types for a maximum number of radio sources.

7. ESTIMATING VERSIONS OF CORRECTIONS IN THE QUALITY OF PERFORMING THE RESEARCH PROGRAM OF THE SPACECRAFT FLIGHT

For a qualitative comparison of versions of a spacecraft flight trajectory, which will be obtained after correction, in terms of the efficiency of implementing the

[1] See [1] and the RadioAstron *User Manual* <http://www.asc.rssi.ru/radioastron/documents/rauh/en/rauh.pdf>.

[2] See <http://www.aoc.nrao.edu/software/sched>.

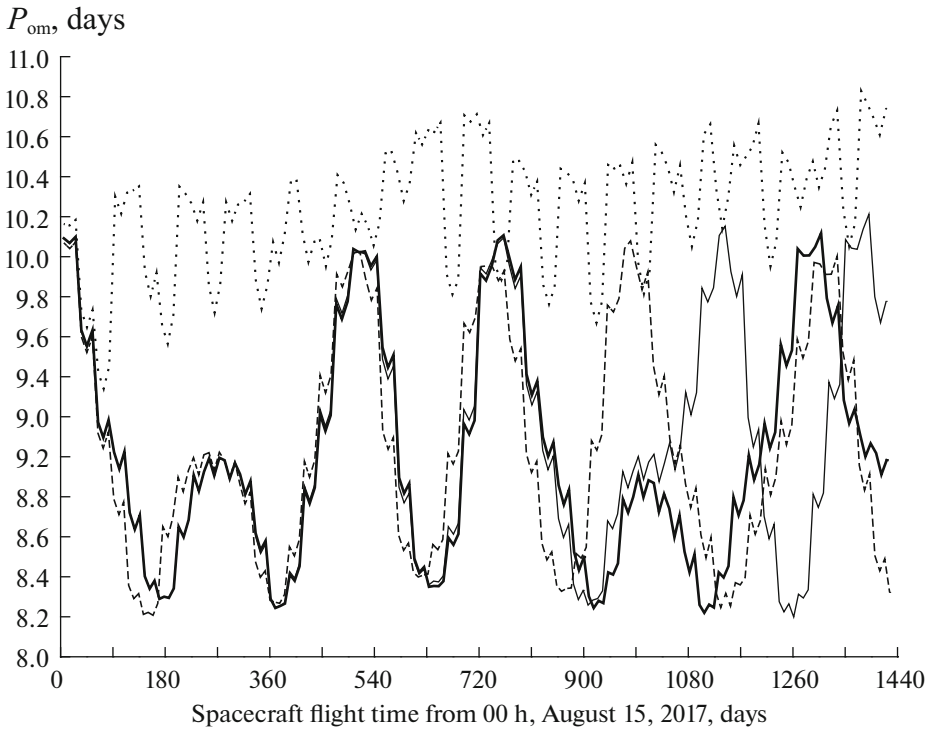

Fig. 13.

further research program of the mission, the list was formed that contains 69 radio sources. These objects were selected from a number of sources declared for observations with using the GSI in the AO4 cycle (July 2016–June 2017). These radio sources are assumed to represent a typical sample of observations that use the GSI. The list includes both radio sources, which are concentrated near the Galaxy plane (pulsars and masers), and extragalactic objects (active cores of galaxies and megamasers). The latter do not have a region of preferential concentration on the sky, though the sample declared for observations has a deficit of objects in the Southern Hemisphere.

For the indicated radio sources, we calculated the tables with the visibility conditions for September 2017–December 2019, for each of the four versions of orbit correction. With the fulfillment of the visibility conditions for the selected sources, we analyzed the parameters that characterize the efficiency of the operation of the ground-space interferometer. The basic parameter is the base's vector projection on the special plane called the *UV* plane. The notions of the GSI base vector, the *UV* plane and the base vector projection (on the *UV* plane) are defined as follows.

The vector of the GSI base is the vector with an origin at the point of location of the ground-based radio telescope, and the end is located at the spacecraft CM at which the space radio telescope is situated.

The UV plane is the reference plane (for the *Ouv* coordinate system (CS)) coinciding with the picture plane, which is orthogonal to the direction from the Earth CM to the radio source. For convenience, the *Ov* axis of the *Ouv* coordinate system is directed along the projection of the angular velocity of Earth rotation around its axis on the picture plane. The *Ou* axis of this system is directed such that, if one looks along it, the

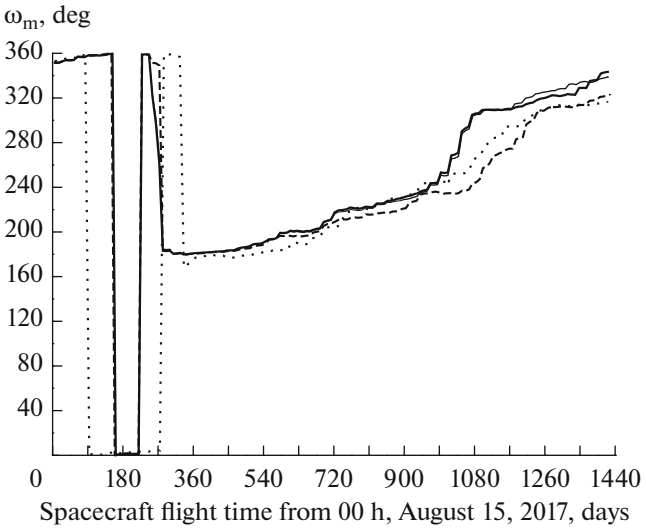

Fig. 14.

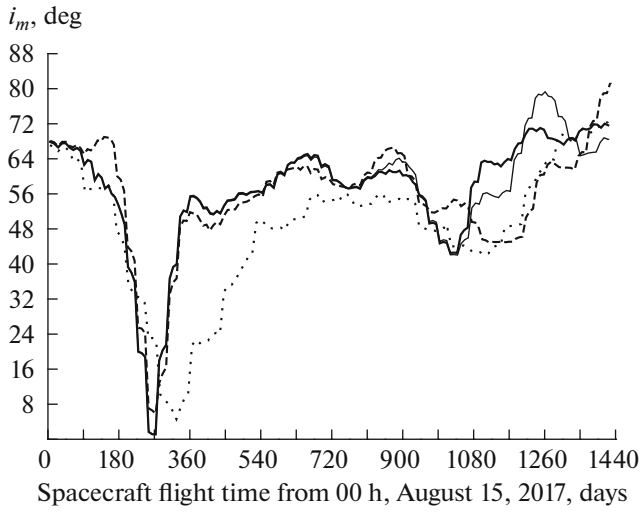

Fig. 15.

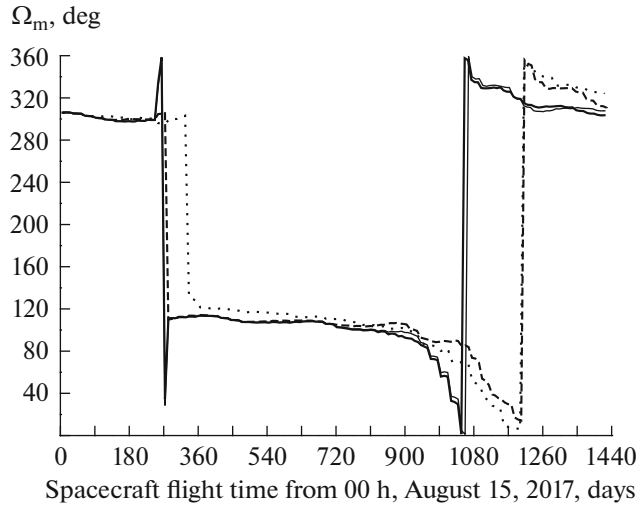

Fig. 16.

direction to the radio source can be combined with the direction of the Ov axis by turning it counterclockwise by a 90° angle. In our presentation below, for brevity, we will also refer to the length of the base vector projection on the *UV* plane as the interferometer base.

In the interferometry, the quality of restoration of the radio source image and the properties of a synthesized directivity pattern are characterized by the *UV* plane coverage with points, each of which represents the end of the base vector projection at a particular time instant of modeled observations [25]. The denser and more uniform the *UV* plane coverage with points, the better it will be. The comparison of *UV* plane coverages between each other was performed by visualized analysis.

Figure 17 shows the examples of *UV* plane coverage for the NGC3079 galaxy during the spacecraft flight from September 2017 to December 2019 after the scheduled performance of correction in two versions, i.e., *K21* (left) and *K23* (right). In this figure, the (*U, V*) components of the base vector projection in the *Ouv* CS are expressed in diameters (D_E) of the Earth, $D_E = 2R_E$ (the value of quantity R_E was presented above). The scale chosen for the *U* and *V* coordinates is convenient in studying the space source using the GSI. It is hard to give unambiguous preference to one of the versions of corrections based on the appearance of coverages of the *UV* plane. Approximately the same properties are inherent in the coatings of the *UV* plane for the other sources from the number of 69 subjected to similar analysis.

For this reason, some integral characteristics were calculated, including T_Σ is the total time accessible for observation using the space telescope and ignoring the time for cooling and N_v is the number of possible versions of 1-h observations that can be carried out for the radio sources from the chosen list. As a rule, at each time instant there exists the choice from several observable radio sources. If at the analyzed time instant this choice is greater, then the number of possible observation versions will also be greater. In the calculations under consideration the time step was one hour. In reality, only one of possible versions will be chosen in the real observation program;

$B_{min}, B_{med}, B_{max}$ are the ranges of values of ground-space bases: minimum, median and maximum, respectively; N_{l2d} is the number of radio sources for which the observations on small bases (less than 2 diameters of the Earth) can be implemented; T_{l2d} is the total time of observations of radio sources, for which the observations on small bases can be implemented; N_{g25d} is the number of radio sources for which the observations on large bases (exceeding 25 Earth diameters) can be implemented; and T_{g25d} is the total time of observations of radio sources for which the observations on large bases can be implemented.

The numerical results of the performed analysis are presented in Table 2 and are illustrated in Fig. 18, which presents histograms of the distribution of the number *N* of possible observation versions depending on the implemented GSI base (*B*) expressed in the Earth diameters. The number of principally possible observation versions was calculated for September 2017–December 2019. Figure 18 shows a histogram of N for corrections of the spacecraft flight trajectory, i.e., version *K21* (May 2017) on the left and version *K23* (July 2017) on the left.

All four versions of the spacecraft flight trajectory correction are acceptable. Each of these versions provides the conditions for observing space radio sources in the range of small to large bases. However, the opportunities for these observations are different. The first version, *K21*, compared to three subsequent versions, provides much more opportunities for observa-

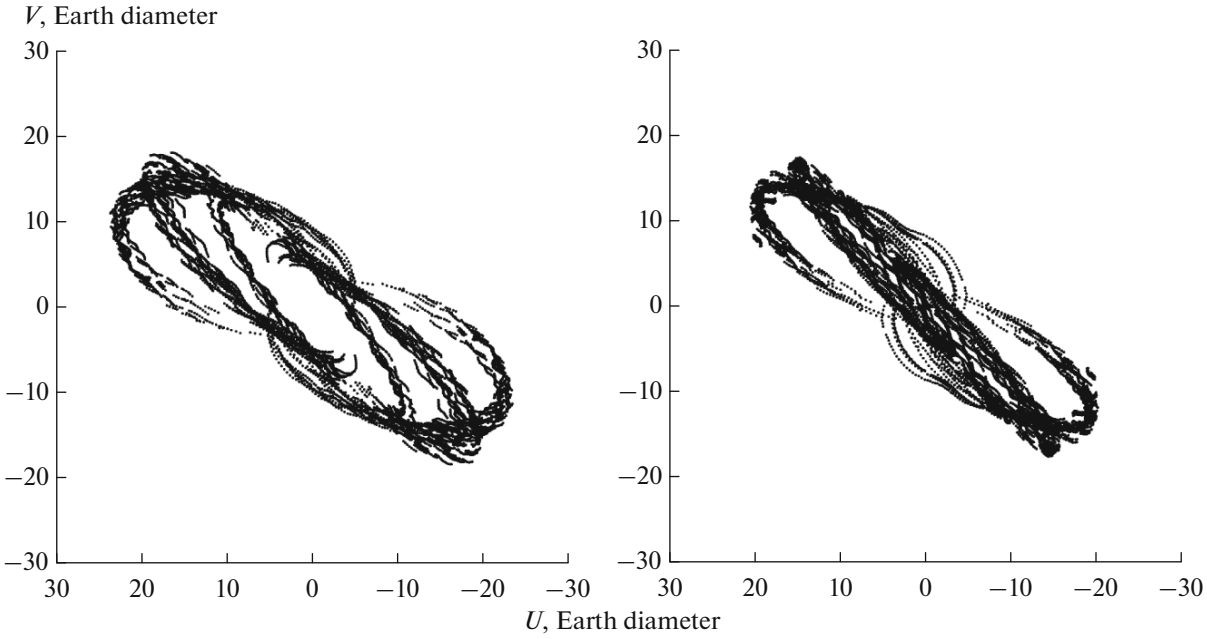

Fig. 17.

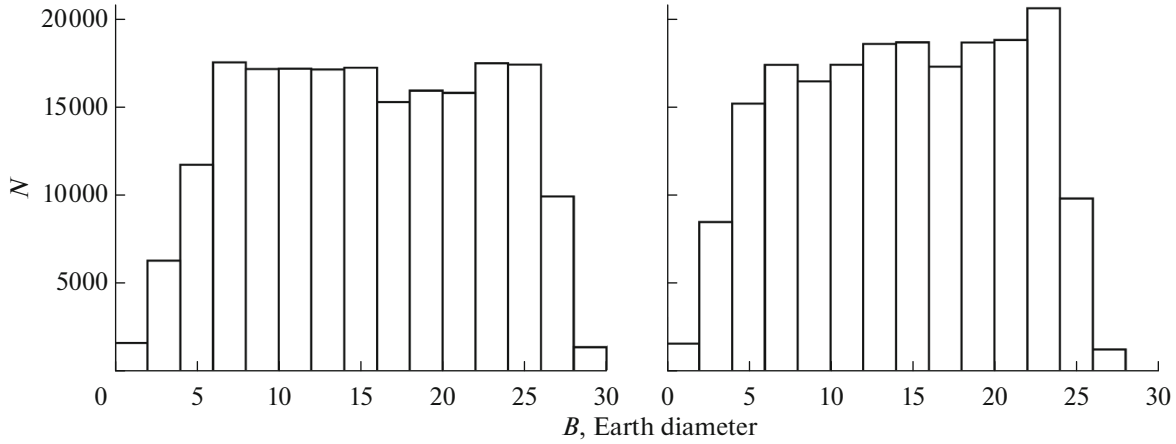

Fig. 18.

tion on extremely large bases due to the decrease in the number of sources visible on small bases and the decrease in the total time acceptable for observations. The last two versions, *K23* and *K24*, seem to be almost equivalent, whereas the *K22* version provides fewer opportunities for observations on small bases. The *K23* version seems to be most optimum, since it provides wide opportunities to construct images using observations on small bases and, at the same time, conserves diverse opportunities for observations on large bases. Similar to *K23*, the *K24* version may be reserved for an emergency situation when performing the *K23* correction. In addition, the correction in July 2017 (the *K23* version) will not require a change in the program of observations in the RadioAstron project, including the program composed before June 2017.

CONCLUSIONS

The studies presented in this paper confirm the need to correct the flight trajectory of the *Spektr-R* spacecraft in 2017.

It has been shown that, beginning in mid-2017 and continuing to the end of 2019, the *Spektr-R* spacecraft will be repeatedly immersed into the Moon's sphere of influence. An algorithm has been developed that

Table 2. Results of analyzing the possible observability of radio sources in September 2017–December 2019 after the nominal performance of considered versions of correcting the spacecraft flight trajectory

Correction	T_Σ, h	N_v, h	$B_{\min}$	B_{med}	$B_{\max}$	N_{l2d}	T_{l2d}, h	N_{g25d}	T_{g25d}, h
K21	9255	199944	0.0	15.2	29.8	55	1484	36	1904
K22	9575	204246	0.0	14.5	27.8	59	1486	27	653
K23	9561	202064	0.0	14.5	27.7	68	1487	26	588
K24	9543	201549	0.1	14.5	27.7	68	1443	29	622

allows one to justify the choice of its performance scheme in the presence of the indicated conditions of encountering the Moon long before performing the correction of the spacecraft flight trajectory.

The scheme of performing the spacecraft flight trajectory correction in 2017 has been substantiated. At first, an attempt will be made to implement the correction (*K23*) by a single actuation of the onboard PS at the middle of July 2017. If this does not happen for any reason, the backup correction (*K24*) will be performed by igniting a PS in the middle of the first ten days of August 2017. The preliminary characteristics of these corrections are presented in Table 1.

REFERENCES

1. Kardashev, N.S., Khartov, V.V., Abramov, V.V., et al., "RadioAstron"-A telescope with a size of 300000 km: Main parameters and first observational results *Astron. Rep.*, 2013, vol. 57, no. 3, pp. 153–194.
2. Andreyanov, V.V., Kardashev, N.S., and Khartov, V.V., Space–ground radio interferometer RadioAstron, *Cosmic Res.*, 2014, vol. 52, no. 5, pp. 319–325.
3. Khartov, V.V., Shirshakov, A.E., Artyukhov, M.I., et al., Features of RadioAstron mission control, *Cosmic Res.*, 2014, vol. 52, no. 5, pp. 326–331.
4. Kardashev, N.S., Kreisman, B.B., Pogodin, A.V., et al., Orbit design for the *Spektr-R* spacecraft of the ground–space interferometer, *Cosmic Res.*, 2014, vol. 52, no. 5, pp. 332–341.
5. Zaslavskii, G.S., Zakhvatkin, M.V., Stepan'yants, V.A., et al., Ballistic and navigation support for the *Spektr-R* spacecraft flight, *Kosm. Raketostroenie*, 2014, vol. 74, no. 1, pp. 15–29.
6. Zaslavskii, G.S., Stepan'yants, V.A., Tuchin, A.G., et al., Trajectory correction of the *Spektr-R* spacecraft motion, *Cosmic Res.*, 2014, vol. 52, no. 5, pp. 353–364.
7. Zaslavskii, G.S., Zakhvatkin, M.V., Stepan'yants, V.A., et al., Ballistic and navigation support for spacecraft flight control and science performance of the RadioAstron project: Five years of flights, *Vestn. NPO im. Lavochkina*, 2016, vol. 33, no. 3, pp. 25–37.
8. Smirnova, T.V., Popov, M.V., Kardashev, N.S., et al., RadioAstron studies of the nearby, turbulent interstellar plasma with the longest space–ground interferometer baseline, *Astrophys. J.*, 2017, vol. 786, pp. 115–128.
9. Biryukov, A.V., Kauts, V.L., Kulagin, V.V., et al., Gravitational redshift test with the space radio telescope"RadioAstron", *Astron. Rep.*, 2014, vol. 58, no. 11, pp. 783–795.
10. Lobanov, A.P., Gómez, J.L., Kovalev, Y.Y., et al., RadioAstron space VLBI imaging of polarized radio emission in the high-redshift quasar 0642+449 at 1.6 GHz, *Astron. Astrophys.*, 2015, vol. 583, A100.
11. Gómez, J.L., Kovalev, Y.Y., Sokolovsky, K.V., et al., Probing the innermost regions of AGN jets and their magnetic fields with RadioAstron. I. Imaging BL Lacertae at 21 microarcsecond resolution, *Astrophys. J.*, 2016, vol. 817, no. 2, p. 96.
12. Kovalev, Y.Y., Kardashev, N.S., Kellermann, K.I., et al., RadioAstron observations of the quasar 3C273: A challenge to the brightness temperature limit, *Astrophys. J. Lett.*, 2016, vol. 820, no. 1, L9.
13. Johnson, M.D., Kovalev, Y.Y., Gurvits, L.I., et al., Extreme brightness temperatures and refractive substructure in 3C273 with RadioAstron, *Astrophys. J. Lett.*, 2016, vol. 820, no. 1, L10.
14. Rudnitskii, A.G., Karuppusamy, R., Popov, M.V., and Soglasnov, V.A., Studies of cosmic plasma using RadioAstron VLBI observations of giant pulses of the pulsar B0531+21, *Astron. Rep.*, 2016, vol. 60, no. 2, pp. 211–219.
15. Gwinn, C.R., Popov, M.V., Kardashev, N.S., et al., PSR B0329+54: Statistics of substructure discovered within the scattering disk on RadioAstron baselines of up to 235,000 km, *Astrophys. J.*, 2016, vol. 822, no. 2, 96.
16. Popov, M.V., Andrianov, A.S., Bartel, N., et al., Distribution of inhomogeneities in the interstellar plasma in the directions of three distant pulsars from observations with the RadioAstron ground–space interferometer, *Astron. Rep.*, 2016, vol. 60, no. 9, pp. 792–806.
17. Kardashev, N.S., Artyukhov, M.I., Kovalev, Yu.Yu., et al., RadioAstron: Results of the science program of 5-year flights, *Vestn. NPO im. S. A. Lavochkina*, 2016, no. 3, pp. 4–24.

18. Popov, M.V., Bartel, N., Kardashev, N.S., et al., PSR B0329+54: Substructure in the scatter-broadened image discovered with RadioAstron on baselines up to 330,000 km, *Mon. Not. R. Astron. Soc.*, 2017, vol. 465, no. 1, pp. 978–985.

19. Popov, M.V., Rudnitskii, A.G., and Soglasnov, V.A., Giant pulses of the Crab Nebula pulsar as an indicator of a strong electromagnetic wave, *Astron. Rep.*, 2017, vol. 61, pp. 178–186.

20. *Navigatsiya kosmicheskikh apparatov pri issledovanii dal'nego kosmosa* (Space Vehicle Navigation in Deep Space Research), Molotov, E.P. and Tuchin, A.G., Eds., Moscow: Radiotekhnika, 2016.

21. Akim, E.L., Zaslavskii, G.S., Stepan'yants, V.A., et al., *Mashinostroenie. Entsiklopediya. Raketno-kosmicheskaya tekhnika* (Machine Building. Encyclopedia. Space Rocket Technology) Legostaev, V.P., Ed., Moscow: Mashinostroenie, 2012.

22. Akim, E.L., Appazov, R.F., Bazhinov, I.K., et al., *Navigatsionnoe obespechenie poleta orbital'nogo kompleksa "Salyut-6"–"Soyuz"–"Progress"* (Navigation Support of the Flight of the "Salyut-6"–"Soyuz"–"Progress" Orbital System), Moscow: Nauka, 1985.

23. Abalakin, V.K., Aksenov, E.P., Grebenikov, E.A., and Ryabov, Yu.A., *Spravochnoe rukovodstvo po nebesnoi mekhanike i astrodinamike* (Guide to Celestial Mechanics and Astrodynamics), Duboshin, G.N., Ed., Moscow: Nauka, 1971.

24. Zhuravlev, V.I., Fakerat software in the international interferometric RadioAstron project with very long ground–space bases, *Cosmic Res.*, 2015, vol. 53, no. 3, pp. 216–225.

25. Tompson, A.R., Moran, J.M., and Svenson, G.W., *Interferometry and Synthesis in Radio Astronomy*, New York: Wiley, 2001, pp. 304–382; Moscow: Fizmatlit, 2003, pp. 276–341.

Translated by Yu. Preobrazhensky